Giant dipole plasmon resonance in fluorene (C$_{13}$H$_{10}$) molecules

Chandan Bagdia [ORCID],[1] Abhijeet Bhogale,[1] László Gulyás,[2] and Lokesh C. Tribedi [ORCID][1,*]

[1]*Department of Nuclear and Atomic Physics, Tata Institute of Fundamental Research, Mumbai 400005, India*
[2]*Institute for Nuclear Research, Debrecen 4001, Hungary*

We report the observation of the giant dipole plasmon resonance in the fluorene molecule (C$_{13}$H$_{10}$), a polycyclic aromatic hydrocarbon, upon collisions with H-like silicon ions. An idea of using highly charged ions to create a large perturbation strength is exploited to observe the plasmon state effectively in the electron double-differential distribution. The signature of plasmon excitation is observed directly as a characteristic broad peak in the electron double-differential spectrum. Such an excited state could not be observed for the same molecule when the low charged ions having lower perturbation were used. This is explained by a model based on dipole approximation and linear response theory for the giant plasmon resonance. The angular distribution of these electrons is modeled using the photoelectron angular distribution for an oscillating dipole superimposed with the postcollision interaction due to the long-range Coulomb interaction between the plasmon electrons and the receding projectile ions.

The knowledge of atoms and molecules has played a crucial role in understanding the universe, particularly in exploring the interstellar medium (ISM) [1]. The polycyclic aromatic hydrocarbons (PAHs) are a class of molecule that has been established to be present in the ISM based on the observed infrared emission spectra [2–4]. A large abundance of the PAHs has been found in Titan's upper environment [5]. Also, the first interstellar detection of an individual PAH, indene (c-C$_9$H$_8$), has been reported only this year [6]. The theoretical and experimental studies involving PAHs have attracted a great deal of attention recently due to their importance in astrophysics and astrochemistry.

The PAHs are, in general, planar molecules having multiple benzoidal rings. They have a delocalized π-electron cloud which provides extra stability in the harsh interstellar medium. These delocalized electrons are highly correlated and can oscillate collectively upon external perturbation. Such collective oscillation of electrons is also known as giant plasmon resonance. The famous bump on the extinction curve at 217.5 nm has been predicted to be due to the plasmon resonances in PAHs [7]. Giant resonances are a very important phenomenon in physics appearing over a wide range of length scales. For example, the giant resonance results in nucleon oscillations [8]; in large atoms, such as $4d \rightarrow \epsilon f$ excitation in Xe and I [9]; in large molecules, such as fullerenes, and C nanotubes [10,11]; and in larger systems, such as metal clusters, nanodots, and solids [12]. Recently, the role of giant dipole resonance in the enhancement of the low-energy electron emission in metal nanoparticle inserted in DNA has been studied theoretically [13]. This aspect of radiosensitization has been investigated experimentally for the iodine-based molecule iodouracil [14].

The contribution of multielectron correlations is challenging to take into account in the theoretical calculations, thereby making these PAH molecules as benchmark systems for the theoretical frameworks which take correlations into account and thus making these studies important from the fundamental molecular physics point of view as well. The PAH molecules are also a subject of interest from a technological perspective. For example, these molecules make a good choice for better plasmonic devices due to their tunability and wider spectral range of operation [15].

The deexcitation of giant dipole plasmon resonance (GDPR) primarily proceeds via electron emission [12]. The differential measurement of these electrons can provide an important understanding of the giant resonances; e.g., the multipole excitation can be probed looking into the angular distributions. Even though the electron emission is a primary channel of deexcitation, the GDPR in PAHs has not been studied extensively in this channel as it is well known that the ion impact electron emission cross sections due to Coulomb ionization are quite large for the lowest-energy electrons, i.e., around 0–30 eV. The electrons emitted following the GDPR fall within this energy range and are hence difficult to distinguish from the background spectrum of the Coulomb ionization. Also, the oscillator strength in the case of smaller PAHs such as fluorene (C$_{13}$H$_{10}$) is small compared to coronene (C$_{24}$H$_{12}$), fullerenes (C$_{60}$ and C$_{70}$), and nanoparticles. Hence, the observation of giant plasmon resonance for PAHs is relatively difficult. Here we have made use of a technique to excite and study the giant plasmon resonance effectively by choosing the highly charged ions as a probe. The GDPR cross section happens to reveal a nearly linear dependence on the projectile charge state, q_p, in the chosen energy range. This was predicted by a model developed for the fullerene molecule [16] as well as observed experimentally [17,18]. Also, it has been observed that the Coulomb ionization cross sections,
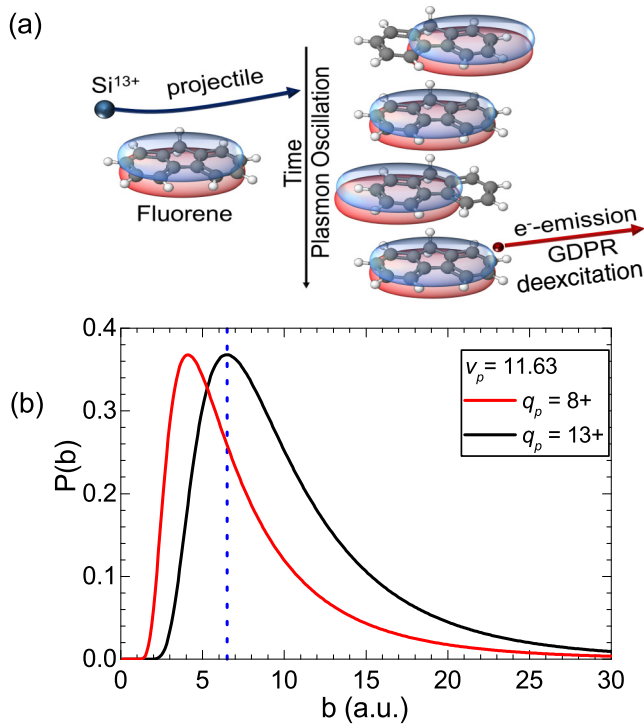
*lokesh@tifr.res.in; ltribedi@gmail.com

FIG. 1. (a) Experimental scheme in which the projectile ions perturb the system and the electron cloud (red and blue circles depict above and below the ionic cage) collectively oscillates, which then predominantly decays via the electron emission (not to scale). (b) The GDPR plasmon excitation probability $P(b)$ as a function of impact parameter b for 94-MeV Si ions ($v_p = 11.63$ a.u.) having 8+ and 13+ charge states. The dotted line shows impact parameter corresponding to the radius of the fluorene molecule ($\sim$6.5 a.u.).

which provides the background under a plasmon peak, reveal a near saturation as a function of q_p [19–21]. Hence, with the saturating background Coulomb ionization cross sections and the enhancing plasmon excitation, the highly charged ions make a suitable choice to study the GDPR in the PAHs.

There have been several works studying the ion impact fragmentation of PAH molecules [22–28]. However, articles investigating the electron emissions upon ion impact from the PAH molecules are scarce [29,30]. More specifically, a few ion impact fragmentation or electron emission studies involving the fluorene ($C_{13}H_{10}$) molecules exist in the literature [30–32].

The fluorene ($C_{13}H_{10}$) molecules have two benzoidal rings connected by a pentagonal ring [see Fig. 1(a)]. The PAH molecules with a pentagonal ring hold particular importance in terms of the formation of the fullerene in the ISM via the PAH processing in a bottom-up mechanism. The fluorenyl cation ($C_{13}H_9^+$) produced upon one hydrogen loss from the fluorene molecule is also a fragmentation product of many other PAHs, making it relevant for the grand-PAH hypothesis, which predicts that the fragmentation of various PAHs would lead to the limited species of stable intermediates [33].

Our primary aim is to investigate the plasmon excitation in the fluorene ($C_{13}H_{10}$) molecules in the electron emission channel. The scheme of the experiment is shown in Fig. 1(a) (not to scale). The projectile ions perturb the system and the

electron cloud collectively oscillates, which then predominantly decays via the e^- emission. These ejected electrons are measured to observe the plasmon resonance. The GDPR model, proposed by Lebrun *et al.*, under the framework of linear response theory and dipole approximation, has been successfully employed for C_{60} molecules [16]. By extending the same model to the fluorene molecule one can see that the plasmon excitation probability for 8+ ions peaks well below the fluorene radial distance (6.5 a.u.) [Fig. 1(b)]. This implies that the ions interact with the individual atoms giving rise to molecular fragmentations, etc. This explains why it is difficult to observe the plasmon excitation of the whole molecule with projectile ions having charge states 8+ [30,32]. However, for 13+ ions, the maximum nearly coincides with the radial distance, suggesting that the ions with the 13+ charge state could excite the GDPR more effectively in such distant collisions with the entire molecule [Fig. 1(b)]. Hence, the experiments are performed using 94-MeV (3.36-MeV/u) Si^{13+} ion beams, obtained from the 14-MV Pelletron accelerator at TIFR, Mumbai. The electrons ejected upon interaction with the effusive jet of fluorene molecules are energy analyzed using an electrostatic hemispherical spectrometer. A separate measurement has also been performed with the CH_4 molecules under the static gas-pressure condition in order to compare with the low-energy spectrum and also for normalization purposes. Further experimental details including the normalization procedure can be found in [32,34,35]. The total uncertainty in the measurement is estimated to be between 20% and 23%, resulting from the uncertainties due to counting statistics (5–10 %), density fluctuation (10%), and the normalization procedure (15%).

The continuum distorted wave with an eikonal initial state (CDW-EIS) model is a first-order distorted wave method introduced for describing ionizing collisions of atoms at medium and high impact energies [36,37]. Extensions of the model to molecular collisions have been provided in [38,39], where the reliability of the method for describing various cross sections was presented for the case of CH_4 molecule. Here we give only a brief description of the theory relevant for the present study with the $C_{13}H_{10}$ molecule. One active electron is considered during the collision which is moving in the combined field of the heavy nuclei and the frozen spectator electrons. The $C_{13}H_{10}$ molecule has 44 orbitals filled with two electrons. However, considering only the valence orbitals and performing the single-center expansion of the multicenter molecular wave functions still requires considerable computational effort that we wanted to avoid in the present treatment. Therefore, our description of the molecule relies on a simpler approximation, known as complete neglect of differential overlap (CNDO), where only the gross feature of the electron-electron interaction is included [40]. In the CNDO approximation the molecular orbitals can be represented in terms of the corresponding atomic orbitals of the constituent atoms. As a result, the double-differential cross section (DDCS) for a given molecular orbital is obtained as a linear combination of atomic DDCSs, where the combination coefficients are obtained from the Mulliken population analysis provided by the GAUSSIAN 09 software package [41]. To check the accuracy of the DDCSs obtained on the CNDO description of the molecular orbitals, we evaluated DDCSs
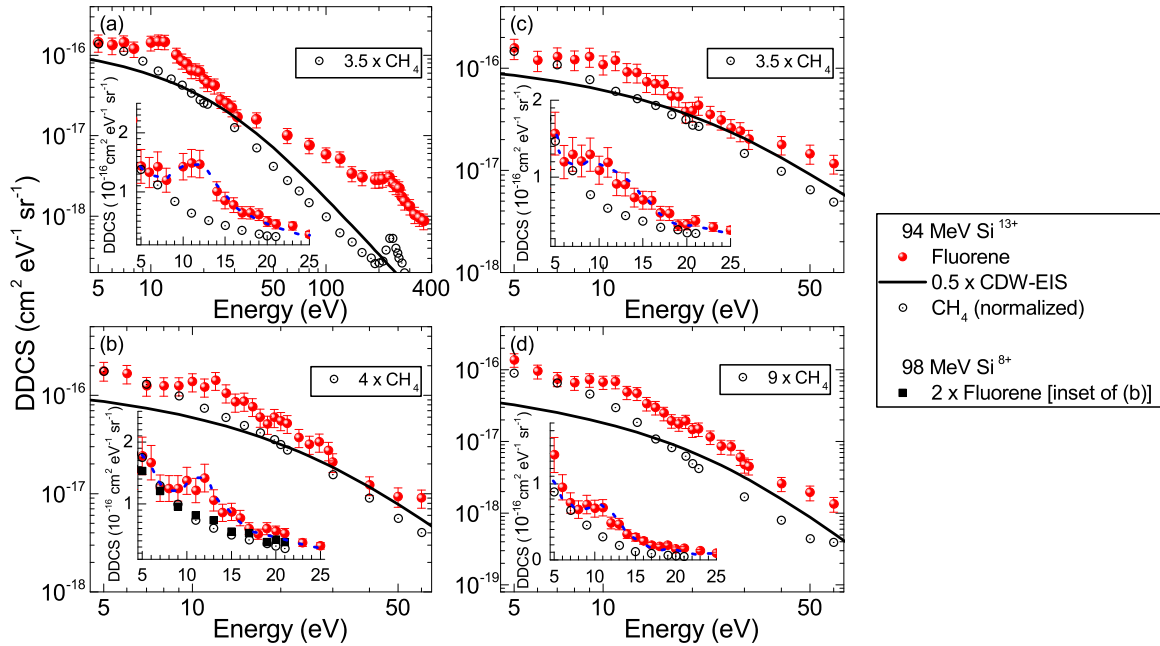
FIG. 2. Energy distributions of the DDCS at particular angles for 94-MeV Si^{13+}: (a) $\theta = 30°$, (b) $\theta = 45°$, (c) $\theta = 60°$, and (d) $\theta = 160°$. Closed (red) circles and open circles represent the $C_{13}H_{10}$ and CH_4 data, respectively. The solid lines represent the CDW-EIS calculations for fluorene. The insets display the DDCS in linear scale and dashed lines are a guide to the eye. The black square in the inset of (d) shows the data for the 98-MeV Si^{8+} ion on fluorene [32]. The CH_4 data are multiplied by suitable factors for comparison only, as indicated in each panel.

for several electron energies (7, 15, and 21 eV), where the single-center expansion of the multicenter molecular orbitals are performed [see Eqs. (4)–(8) in [38]]. These DDCS results are very close to the ones obtained with the CNDO molecular description.

The energy distributions of the e^- DDCS for fluorene molecules upon 94-MeV Si^{13+} ion impact are shown for four different angles in Figs. 2(a)–2(d). The results measured for CH_4, along with the CDW-EIS calculations, are also shown. The cross sections fall by a few orders of magnitude in the emitted electron energy range of 5–400 eV [for example, see Fig. 2(a)], which is quite typical in ion-atom collisions. The C *KLL* Auger electrons are observed in the spectrum as a peak at an energy of about 240 eV [Fig. 2(a)]. Similar measurements in the case of the Si^{8+} ion impact, having nearly the same velocity, show a smooth continuum in the lower-energy part in which the plasmon peak is not observed [inset of Fig. 2(b)] [32]. The spectrum obtained for CH_4 molecules also shows a similar smooth continuum spectrum. However, for the Si^{13+} projectile ions on fluorene, a clear broad hump is observed in the energy range of 6–17 eV. The inset shows a plot in linear scale. This hump corresponds to the giant plasmon excitation in the fluorene molecules. The electrons ejected upon plasmon excitation would have to overcome the ionization potential. Therefore, the observed electron energy would be the difference between the plasmon excitation energy and the ionization potential. The observed peak position for the hump is 10–11 eV, which corresponds to the giant plasmon excitation energy of 18–19 eV since the first ionization potential for fluorene is 7.91 eV. The observed plasmon excitation energy is in reasonably good agreement with the reported tabulated excitation energies [42]. In that study, the peak in the photoion yield was tabulated at a photon energy of 17.1 eV for singly

ionized fluorene and at 17.8 eV for one H-loss fluorene cation. Also, we observe a peak width of about 4–6 eV, which in the case of the C_{60} is observed to be about 10–12 eV [11] and for coronene about 7–8 eV [29].

For large molecules such as fullerene (C_{60}) and coronene ($C_{24}H_{12}$), the GDPR was observed using ion beams having a lower charge state, F^{9+} and O^{8+}, respectively, since the oscillator strength is large [11,29]. However, for the fluorene ($C_{13}H_{10}$) molecules having smaller oscillator strength, the ions with a higher charge state, Si^{13+}, excite the GDPR effectively. Therefore, the use of ions with a higher charge, i.e., higher perturbation strength, is a promising choice to excite and study the plasmon in molecules with smaller oscillator strengths.

The angular distributions at four representative electron energies in the angular range of $20°-160°$ are plotted in Fig. 3. The measured angular distributions for the fluorene are shown along with the measured data for CH_4 and the CDW-EIS calculations for the purpose of comparison. The angular distributions of the electrons away from the GDPR peak (i.e., greater than or equal to 20 eV) are shown for two representative energies of 40 and 60 eV. The angular distribution shows a peak around the ejection angle of about $80°$ which arises due to the binary encounter nature of the collisions. Also, a forward-backward asymmetry is observed in the electron emission which arises from the postcollision interaction (PCI) of the ejected electrons with the residual target and the projectile. These features of ion-atom or ion-molecule collisions are well understood and very well reproduced by the CDW-EIS model calculations. The angular distribution of the electrons in the GDPR peak region (i.e., 6–17 eV) is shown for two energies of 10 and 13 eV. In the case of the fluorene molecules, the cross section goes via a dip and then shows an increasing
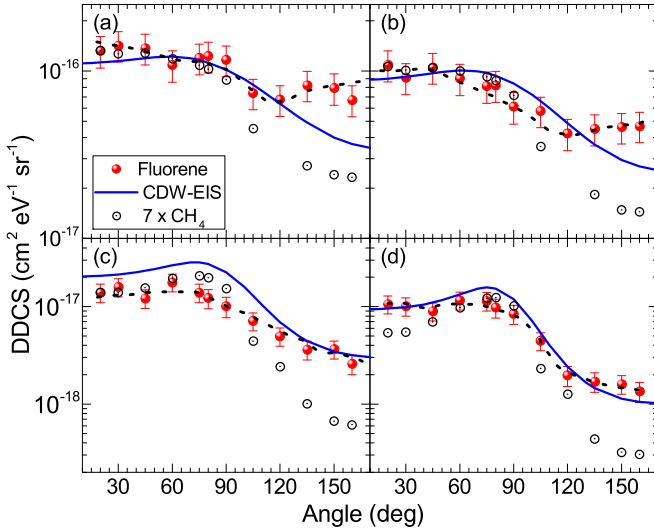
FIG. 3. Angular distributions of the DDCS of the ejected electrons for the fluorene (closed circles), CH_4 (open circles with dots), and CDW-EIS calculations (solid lines) in collisions with 94-MeV Si^{13+} ions at (a) 10 eV, (b) 13 eV, (c) 40 eV, and (d) 60 eV. The dashed lines are a guide to the eye.
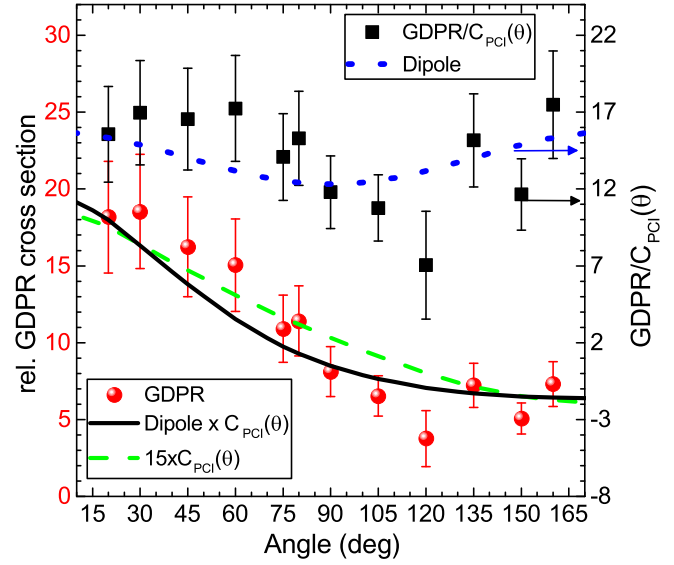

FIG. 4. Angular distribution of the $d\sigma_{pl}^{exp}/d\Omega$ for plasmon electrons, denoted as relative GDPR cross section [experiment (closed circles)], with the scale on the left axis. The scaled PCI correction factor [$C_{PCI}(\theta)$], with the numbers on the left axis, is shown as dashed green line. The oscillating dipole distribution including the PCI correction factor (i.e. Eq. (2)) is indicated as solid black line, with the scale on the left axis. The plasmon electron angular distribution corrected for the PCI effect [i.e. $(d\sigma_{pl}^{exp}/d\Omega)/C_{PCI}(\theta)$] is shown as closed square symbols with the scale on the right axis. Angular distribution for the oscillating dipole i.e. Eq. (1) is indicated as dotted blue line, with the scale on the right axis.

trend for the backward angles. With respect to the higher emission energies [Figs. 3(c) and 3(d)], for energies centered on the plasmon oscillation [Figs. 3(a) and 3(b)], the increase in cross section in the forward and backward directions is due to the plasmon contribution. There is a clear distinction in the angular distributions of the CH_4 and CDW-EIS model calculations from that of the fluorene molecules.

The plasmon contribution for each angle [i.e. $d\sigma_{pl}^{exp}/d\Omega$] is derived by integrating the area under the plasmon peak and subtracting the Coulomb ionization background contribution. The angular distribution of $d\sigma_{pl}^{exp}/d\Omega$ is plotted in Fig. 4 (as denoted by relative GDPR cross section). As the ion beam passes by the fluorene molecules, it attracts and displaces the electron cloud, which is then pulled back by the restoring force exerted by the ionic cage, therein setting up the collective oscillations of electrons about the ionic cage [see Fig. 1(a)]. This system can be considered as an oscillating dipole. The dipole contribution averaged over all the molecular orientations and the cylindrical symmetry of the collision system results in the effective induced dipole aligned with the beam direction. Hence, the angular distribution is modeled using the photoelectron angular distribution for an oscillating dipole (blue dotted line in Fig. 4). It is given by

$$\frac{d\sigma_{pl}}{d\Omega} = \frac{\sigma_{pl}}{4\pi}[1 + \beta P_2(\cos\theta)], \qquad (1)$$

where σ_{pl} represents the total plasmon cross section, θ is the angle between the ejected electrons and the direction of the dipole, which in this case is the beam direction, β is an anisotropy parameter, and $P_2(\cos\theta) = \frac{1}{2}(3\cos^2\theta - 1)$. In general, for fast ion-atom collisions the asymmetry in the electron emission is highly influenced by the PCI effect. To estimate the contribution by the PCI effect we follow the following procedure. The first Born (B1) calculation is a single-center model considering only the target center effects. Therefore, it

predicts nearly symmetric angular distribution. The CDW-EIS model includes the interaction with both centers (target and projectile) and describes very well the PCI effects. Therefore, the correction in the angular distribution due to the PCI effect is derived, as a factor $C_{PCI}(\theta)$, by taking the ratio of the DDCS for the CDW-EIS model to the B1 calculations at an ejected electron energy of 10 eV (green dashed line in Fig. 4). The $C_{PCI}(\theta)$ is nearly the same for the electron energies in the range of plasmon peak; hence the ratio of the CDW-EIS model to the B1 calculation at 10 eV is used to estimate $C_{PCI}(\theta)$. Finally, the angular distribution is modeled by multiplying the correction factor $C_{PCI}(\theta)$ by the angular distribution given by Eq. (1). Hence, the data are fitted using

$$\frac{d\sigma_{pl}}{d\Omega} = A[1 + \beta P_2(\cos\theta)]C_{PCI}(\theta), \qquad (2)$$

where A is a proportionality constant.

The model described above reproduces the observed angular distribution reasonably well (black solid line in Fig. 4). The value of the anisotropy parameter β is found to be about 0.2 (± 0.12). The observed plasmon angular distribution corrected for the PCI effect (black squares in Fig. 4) along with the angular distribution for the oscillating dipole is also shown in Fig. 4. This model was successfully used to describe the angular distribution of the plasmon electrons emitted from the C_{60} molecules [11].

The energy distribution of the single-differential cross section (SDCS) obtained by integrating over all the angles is
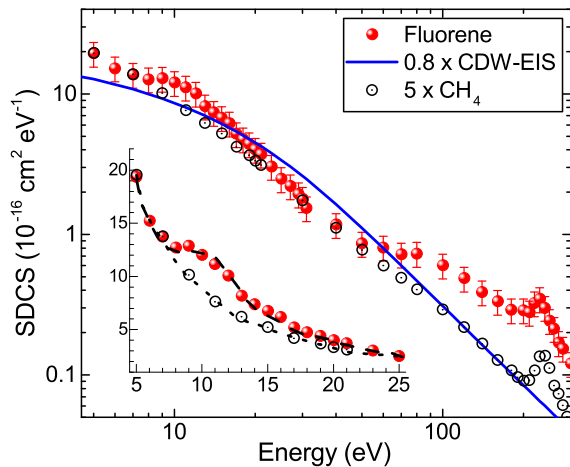
FIG. 5. Energy distribution of the SDCS of the electron emission for the fluorene (closed circles), CH_4 (open circles with dots), and CDW-EIS calculations (solid line). The inset shows a close-up in the linear scale spectrum and the dashed line is a guide to the eye.

plotted in Fig. 5. A broad hump corresponding to GDPR can be observed at 10–11 eV in the SDCS as well. The linear scale plot of the low-energy region with the CH_4 data is shown in the inset. The total plasmon cross section is derived by integrating the angular distribution (red circles in Fig. 4) over all the angles. The measured cross section of GDPR is found to be 1.7×10^{-15} cm^2 and that predicted by the GDPR model is 6.6×10^{-15} cm^2. The overestimation of the cross section by the model could be associated with the use of the higher oscillator strength for the GDPR. We have assumed the oscillator strength to be the number of π electrons, i.e., 12. However, the actual oscillator strength could be less than this value. Also, the GDPR model, which is a perturbative approach, may not be fully accurate since the impact parameter of excitation probability maxima is comparable to the radial distance of fluorene. The value of the fitting parameter

A [in Eq. (2)] times 4π is $(2.26 \pm 0.14) \times 10^{-15}$ cm^2, which is close to the measured total GDPR cross section σ_{pl}, i.e., 1.7×10^{-15} cm^2. The slight difference of a factor of 1.3 arises due to the normalization constant for the $C_{PCI}(\theta)$ [included in A and not shown explicitly in Eq. (2)]. The contribution of the plasmon peak to the total fluorene cross section, obtained by integrating over all the angles and energies, is about 6%. The contribution of the plasmon peak is about 12% of that of the Coulomb ionization cross section in the range of 5–20 eV.

To conclude, the giant plasmon resonance in the fluorene molecule has been observed directly as a characteristic peak in the double-differential electron emission spectrum. A technique of using fast highly charged ions to excite the plasmon has been demonstrated. The GDPR excitation energy has been found to be about 18–19 eV. The angular distribution of the plasmon electrons was modeled by incorporating the correction due to the postcollision effect to the angular distribution of the oscillating dipole. The total plasmon contribution was found to be about 12% of the Coulomb ionization cross section in the range of 5–20 eV. A GDPR model based on the dipole approximation and linear response theory, which was applied for the plasmon oscillation in fullerene, has been shown to reproduce the essential features observed here for the fluorene molecule, at least qualitatively.

[1] A. G. G. M. Tielens, Rev. Mod. Phys. **85**, 1021 (2013).

[2] A. Leger and L. d'Hendecourt, Astron. Astrophys. **146**, 81 (1985).

[3] L. J. Allamandola, D. M. Hudgins, and S. A. Sandford, Astrophys. J. **511**, L115 (1999).

[4] A. Tielens, Annu. Rev. Astron. Astrophys. **46**, 289 (2008).

[5] M. López-Puertas, B. Dinelli, A. Adriani, B. Funke, M. García-Comas, M. Moriconi, E. D'Aversa, C. Boersma, and L. Allamandola, Astrophys. J. **770**, 132 (2013).

[6] A. M. Burkhardt, K. L. K. Lee, P. B. Changala, C. N. Shingledecker, I. R. Cooke, R. A. Loomis, H. Wei, S. B. Charnley, E. Herbst, M. C. McCarthy, and B. A. McGuire, Astrophys. J. Lett. **913**, L18 (2021).

[7] W. W. Duley, Astrophys. J. **639**, L59 (2006).

[8] H. Gove, A. Litherland, and R. Batchelor, Nucl. Phys. **26**, 480 (1961).

[9] D. L. Ederer, Phys. Rev. Lett. **13**, 760 (1964).

[10] G. F. Bertsch, A. Bulgac, D. Tománek, and Y. Wang, Phys. Rev. Lett. **67**, 2690 (1991).

[11] A. H. Kelkar, L. Gulyás, and L. C. Tribedi, Phys. Rev. A **92**, 052708 (2015).

[12] F. Calvayrac, P.-G. Reinhard, E. Suraud, and C. Ullrich, Phys. Rep. **337**, 493 (2000).

[13] A. V. Verkhovtsev, A. V. Korol, and A. V. Solov'yov, Phys. Rev. Lett. **114**, 063401 (2015).

[14] A. Mandal, M. R. Chowdhury, C. Bagdia, J. M. Monti, R. D. Rivarola, P. F. Weck, and L. C. Tribedi, Phys. Rev. A **102**, 062811 (2020).

[15] A. Manjavacas, F. Marchesin, S. Thongrattanasiri, P. Koval, P. Nordlander, D. Sánchez-Portal, and F. J. García de Abajo, ACS Nano **7**, 3635 (2013).

[16] T. LeBrun, H. G. Berry, S. Cheng, R. W. Dunford, H. Esbensen, D. S. Gemmell, E. P. Kanter, and W. Bauer, Phys. Rev. Lett. **72**, 3965 (1994).

[17] A. H. Kelkar, U. Kadhane, D. Misra, L. Gulyas, and L. C. Tribedi, Phys. Rev. A **82**, 043201 (2010).

[18] U. Kadhane, A. Kelkar, D. Misra, A. Kumar, and L. C. Tribedi, Phys. Rev. A **75**, 041201(R) (2007).

[19] S. Bhattacharjee, C. Bagdia, M. R. Chowdhury, J. M. Monti, R. D. Rivarola, and L. C. Tribedi, Eur. Phys. J. D **72**, 15 (2018).

[20] U. Tiwari, A. K. Saha, L. C. Tribedi, M. B. Kurup, P. N. Tandon, and L. Gulyás, Phys. Rev. A **58**, 4494 (1998).

[21] B. Brendlé, R. Gayet, J. P. Rozet, and K. Wohrer, Phys. Rev. Lett. **54**, 2007 (1985).

[22] A. I. S. Holm, H. Zettergren, H. A. B. Johansson, F. Seitz, S. Rosén, H. T. Schmidt, A. Ławicki, J. Rangama, P. Rousseau, M. Capron, R. Maisonny, L. Adoui, A. Méry, B. Manil, B. A. Huber, and H. Cederquist, Phys. Rev. Lett. **105**, 213401 (2010).

[23] A. Ławicki, A. I. S. Holm, P. Rousseau, M. Capron, R. Maisonny, S. Maclot, F. Seitz, H. A. B. Johansson, S. Rosén, H. T. Schmidt, H. Zettergren, B. Manil, L. Adoui, H. Cederquist, and B. A. Huber, Phys. Rev. A **83**, 022704 (2011).

[24] S. Martin, L. Chen, R. Brédy, G. Montagne, C. Ortega, T. Schlathölter, G. Reitsma, and J. Bernard, Phys. Rev. A **85**, 052715 (2012).

[25] J. Postma, S. Bari, R. Hoekstra, A. G. G. M. Tielens, and T. Schlathölter, Astrophys. J. **708**, 435 (2009).

[26] G. Reitsma, H. Zettergren, S. Martin, R. Brédy, L. Chen, J. Bernard, R. Hoekstra, and T. Schlathölter, J. Phys. B **45**, 215201 (2012).

[27] G. Reitsma, H. Zettergren, L. Boschman, E. Bodewits, R. Hoekstra, and T. Schlathölter, J. Phys. B **46**, 245201 (2013).

[28] P. Rousseau, A. Ławicki, A. Holm, M. Capron, R. Maisonny, S. Maclot, E. Lattouf, H. Johansson, F. Seitz, A. Méry, J. Rangama, H. Zettergren, S. Rosén, H. Schmidt, J.-Y. Chesnel, A. Domaracka, B. Manil, L. Adoui, H. Cederquist, and B. Huber, Nucl. Instrum. Methods Phys. Res. B **279**, 140 (2012).

[29] S. Biswas and L. C. Tribedi, Phys. Rev. A **92**, 060701(R) (2015).

[30] S. Biswas, C. Champion, P. Weck, and L. C. Tribedi, Sci. Rep. **7**, 5560 (2017).

[31] C. Bagdia, S. Biswas, A. Mandal, S. Bhattacharjee, and L. C. Tribedi, Eur. Phys. J. D **75**, 37 (2021).

[32] C. Bagdia, A. Mandal, M. R. Chowdhury, S. Bhattacharjee, M. N. Murty, D. Misra, C. Champion, L. Gulyas, P. F. Weck, and L. C. Tribedi, J. Phys. B **54**, 155202 (2021).

[33] H. Andrews, C. Boersma, M. W. Werner, J. Livingston, L. Allamandola, and A. Tielens, Astrophys. J. **807**, 99 (2015).

[34] C. Bagdia, S. Bhattacharjee, M. Roychowdhury, A. Mandal, G. Lapicki, and L. C. Tribedi, X-Ray Spectrom. **49**, 160 (2020).

[35] A. N. Agnihotri, S. Nandi, S. Kasthurirangan, A. Kumar, M. E. Galassi, R. D. Rivarola, C. Champion, and L. C. Tribedi, Phys. Rev. A **87**, 032716 (2013).

[36] D. S. Crothers and L. J. Dubé, Adv. At. Mol. Opt. Phys. **30**, 287 (1992).

[37] N. Stolterfoht, R. D. DuBois, and R. D. Rivaola, *Electron Emission in Heavy Ion Atom Collision* (Springer, Berlin, 1997).

[38] L. Gulyás, I. Tóth, and L. Nagy, J. Phys. B **46**, 075201 (2013).

[39] A. Mandal, C. Bagdia, M. R. Chowdhury, S. Bhattacharjee, D. Misra, J. M. Monti, R. D. Rivarola, and L. C. Tribedi, Phys. Rev. A **101**, 062708 (2020).

[40] J. A. Pople and G. A. Segal, J. Chem. Phys. **44**, 3289 (1966).

[41] M. Frisch, G. W. Trucks, H. B. Schlegel, G. E. Scuseria, M. A. Robb, J. R. Cheeseman, G. Scalmani, V. Barone, B. Mennucci, and G. Petersson, Gaussian 09 (Gaussian, Inc., Wallingford, 2009), revision A.02.

[42] H. Jochims, E. Rühl, H. Baumgärtel, S. Tobita, and S. Leach, Int. J. Mass Spectrom. Ion Process. **167–168**, 35 (1997).